160

The Structure of Controlled Shear Bands in Dynamically Deformed Reactive Mixtures

V.F. NESTERENKO, M.A. MEYERS, H.C. CHEN, and J.C. LaSALVIA

The structure of controlled high-strain-rate shear bands generated in heterogeneous reactive porous materials (Nb + Si, Mo + Si + $MoSi_2$) has been investigated using axially symmetric experimental configurations in which the source of energy is the detonation of low velocity explosives. The deformation was highly localized, with profuse formation of shear bands, which have thicknesses of 5 to 20 μm. The experimental method generated overall strains up to 100 and strain rates $\dot{\gamma}$ of approximately 10^7 s^{-1}. Changes in particle morphology, melting, and regions of partial reaction on three different length scales were observed. The shear band thickness is smaller than the initial characteristic particle size of the porous mixture ($\leq$44 μm), ensuring a cooling time of the deformed material on the same order of magnitude as the deformation time (10^{-5} s). In the shear localization regions, two characteristic phenomena were observed: (a) a shear fracture subdividing the Nb particles into thin parallel layers and (b) the formation of vortices. A mechanism for the reaction inside the shear bands is proposed, and an expression for the largest size of chemical products as a function of shear deformation is obtained.

I. INTRODUCTION

THE shock-wave loading of solids and porous materials results in phase transitions and chemical reactions on a time scale which is much smaller than the one for static conditions, where diffusional processes usually play the main role. The shear deformation and high density of lattice defects are considered to be responsible for this unique behavior.[1,2,3] The qualitative importance of overall shear under quasistatic conditions was first demonstrated by Bridgman.[4] A reaction mechanism based on the continuous generation of a fresh solid (Nb or Mo)-liquid (Si) interface, enabling a high reaction rate, was proposed[5] as a classification of reactions based on their completion during the shock loading process or after its passage.[6,7]

It is difficult to correlate phase transitions, chemical reactions, and shear parameters under shock-wave loading at the macro, meso, and micro levels. Moreover, the amplitude of shock pressure is not the main parameter responsible for fast reaction mechanisms.[7] The thick-walled cylinder method,[8,9,10] which was originally developed for the investigation of deformation and shear localization processes in solid materials (copper, aluminum, stainless steel, and polymers) at high strain rates, was modified for the investigation of these processes in porous materials.[11] It enables the control of overall strain parameters of porous materials under dynamic loading and provides, through localization of shear, extremely small sizes of "samples," ensuring a rapid cooling of the reaction products created as a result of the dynamic deformation.

II. EXPERIMENTAL PROCEDURES

The Nb and Si powders were purchased from Cerac (Milwaukee, WI) and had sizes of -325 mesh ($<$44 μm). These powders were selected because of the previous research in which reaction between Nb and Si under shock compression had been thoroughly investigated.[12,13] The thick-walled cylinder method,[8,9,10] applied to solid materials, was modified to accommodate porous mixtures.

Three experimental configurations were used to generate controlled and prescribed shear localization in porous samples. They are shown in Figure 1. Details of the experimental setup are presented in Figure 2.

In configuration 1 (Figures 1(a) and (b)), a porous 68 wt pct Nb-32 wt pct Si mixture, with a density of 2 g/cm^3 ($\sim$50 pct of theoretical value), was initially placed in a tubular cavity between a central copper rod (16.2-mm diameter) and an outer copper tube (20-mm inner diameter and 30.8-mm outer diameter). An explosive (explosive 1, Figure 1(a)) with a low detonation velocity (2.5 km/s) was used to densify this mixture to a density of 3.2 g/cm^3 ($\sim$75 pct of theoretical value). Detonation was initiated at the top of the charge and propagated along the cylinder axis. No shear localization was observed after this step, because the overall plastic deformation is sufficiently small (final diameter of inner surface of driving copper cylinder is equal to 18.7 mm). This stage only produced the densification of the powder mixture. A cylindrical hole with 11-mm diameter was drilled along the longitudinal axis of the copper rod, and this composite cylinder was collapsed by the detonation of a second cylindrical explosive charge (explosive 2, Figure 1(b)) with a detonation velocity of 4 km/s, an initial density of 1 g/cm^3, and an outer diameter of 60 mm (Figure 2). This second explosive event produced significant plastic deformation in the densified porous layer, which was highly localized in shear bands and not homo-

V.F. NESTERENKO, Professor, on leave from the Lavrentyev Institute of Hydrodynamics, Russian Academy of Sciences, Novosibirsk, 630090, Russia, M.A. MEYERS, Professor, H.C. CHEN, Graduate Student, and J.C. LaSALVIA, Post-Doctoral Fellow are with the Institute for Mechanics and Materials, Department of Applied Mechanics and Engineering Sciences, University of California, San Diego, CA 92093.

This article is based on a presentation made in the symposium "Dynamic Behavior of Materials," presented at the 1994 Fall Meeting of TMS/ASM in Rosemont, Illinois, October 3–5, 1994, under the auspices of the TMS-SMD Mechanical Metallurgy Committee and the ASM-MSD Flow and Fracture Committee.

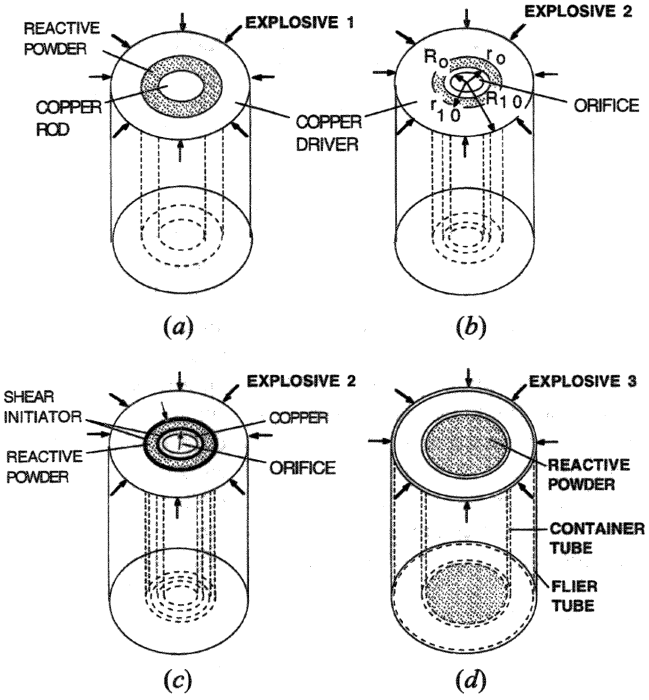

Fig. 1—Geometry and sequence of deformation events in thick-walled cylinder method. Configuration 1: (*a*) initial geometry—densification by explosive 1; and (*b*) powder densified—after drilling of central orifice, cylinder collapsed by explosive 2. Configuration 2: (*c*) cylinder with orifice collapsed by explosive 2 with shear localization assistance by amorphous layer (shown by arrows). Configuration 3: (*d*) use of flier tube.

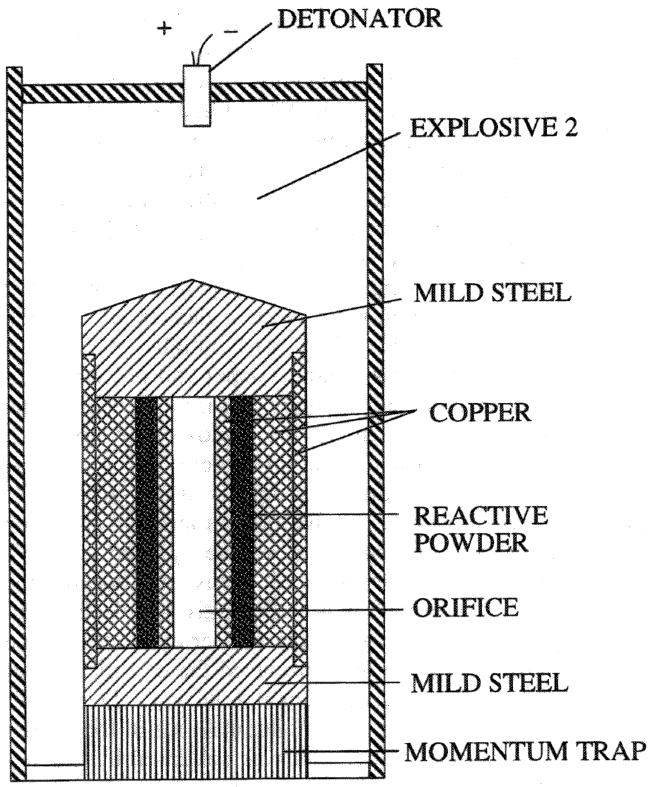

Fig. 2—Overall experimental sketch for configuration 1 (final phase) and configuration 2.

geneously distributed. The average values of r and r_1 (internal and external radii of the porous layer after collapse) were equal to 5.9 and 7.5 mm, respectively. Their initial values are 8.1 mm (r_0) and 9.35 mm (r_{10}).

Configuration 2 (Figure 1(c)) was used for the same powder (initial density 2 g/cm³) as configuration 1. The powder was placed in the tubular cavity with inner and outer diameters 16.4 and 21.7 mm, respectively. A pre-existing hole along the longitudinal axis of assembly, with a diameter of 11 mm, ensured high plastic deformation directly applied to the porous material. A few layers of amorphous ribbon (23-μm thick) were placed along the cylinder walls to initiate shear localization in powder, with a lower density, at an early stage of collapse of the inner hole. It has been established[14] that metallic glass foils undergo shear localization when dynamically deformed in a cylindrical geometry. The average values of r and r_1 after collapse were equal to 6.5 and 8.1 mm and plastic deformation was also highly localized, as in configuration 1.

It is necessary to mention that the explosive parameters in the thick-walled cylinder method (detonation velocity, density, and thickness) were carefully selected to provide a "smooth" pore collapse, by eliminating wave propagation effects and by avoiding fracturing due to the spallation process and the radial cracks which can result from the back movement from the center after collapse. It is also necessary to minimize the effects of jet formation and the trapping of hot air in the center of the collapsing cylinder. The velocity of the inner wall during the collapse process was measured by the electromagnetic gage method.[9]

Configuration 3 was applied to the radial compression of the porous mixture $MoSi_2$ + Mo + Si in a steel container (Figure 1(d)).[15] These powders also had a mesh size of −325 (−44 μm) and an initial density of ~60 pct of the theoretical value. Their deformation was produced by the impact of a steel cylinder driven by an explosive with a detonation velocity of 3.4 km/s, as shown in Figure 1(d). This resulted in an impact velocity of approximately 800 m/s, generating considerable shock pressures within the powders. Shock consolidation of powders using this flyer tube method is described in Reference 15. The formation of spiral surfaces corresponding to maximum stresses and strains is also described.

The porous mixture on the second stage (hole collapse) in configuration 1 deforms practically without change in density, as can be deduced from the initial and final average dimensions of the porous layer. In contrast, in configuration 2, the density is approximately doubled and is close to the solid density of the mixture. It is difficult to determine the radius at which shear localization starts in the porous material. The quantitative determination of the overall porous material strain can be obtained from the strains in the incompressible copper shell driving the collapse process.

The overall radial and tangential engineering strains (e_{rr} and $e_{\varphi\varphi}$) for an incompressible material, before the onset of localization, can be estimated knowing the initial and final radii, ρ_0 and ρ, at a general point:

$$e_{rr} = \frac{\rho_0}{\rho} - 1, \qquad e_{\varphi\varphi} = \frac{\rho}{\rho_0} - 1 \qquad [1]$$

The overall strains in the surfaces of copper cylinders restricting the porous tubular layer can be found from Eq. [1]. The final radii ρ and R (or R_1) and initial radius R_0 (or R_{10}) (Figure 1(b)) are experimentally measured, and the

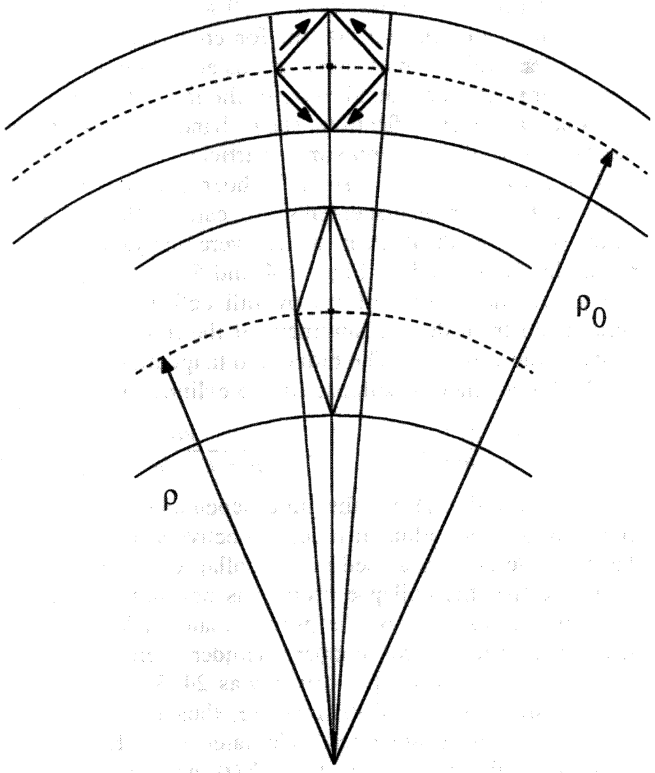

Fig. 3—Geometry of pure shear in incompressible thick-walled cylinder under uniform plastic deformation; ρ_0 and ρ are the initial and final radii of one element, respectively.

value of ρ_0, which corresponds to a preselected value of ρ, can be calculated using Eq. [2]:

$$\rho_0^2 = \rho^2 + R_0^2 - R^2 = \rho^2 + R_{10}^2 - R_1^2 \qquad [2]$$

where R and R_1 are the final radii of the inner hole and outer cylinder surface.

The strain state in cylindrical geometry in the uniformly deformed incompressible material is of pure shear,[16] and the deformation of an element is depicted in Figure 3. This type of shear can be realized by two systems of mutually perpendicular sets of slip planes, in comparison with one system for "simple shear." No rotation is associated with pure shear. In the experiments reported herein, usually only one system of slip planes in a given point of porous mixture was observed. Thus, locally, the state of strain can be of simple shear after shear localization.

The overall strain in copper at the boundary with the porous layer outside the shear localization region can be estimated using Eq. [1]. For configuration 1, after the first explosive event, one obtains at $\rho = r_{10}$, $e_{rr} \approx 0.07$ and $e_{\varphi\varphi} \approx -0.07$. After the second explosive event, one obtains at $\rho = r_1$, $e_{rr} \approx 0.25$ and $e_{\varphi\varphi} \approx -0.2$; and at $\rho = r$, one finds $e_{rr} \approx 0.37$ and $e_{\varphi\varphi} \approx -0.27$. For configuration 2, at $\rho = r_1$, $e_{rr} \approx 0.34$ and $e_{\varphi\varphi} \approx -0.25$; and at $\rho = r$, $e_{rr} \approx 0.26$ and $e_{\varphi\varphi} \approx -0.21$. Note that the deformation in copper under these conditions is homogeneous.[9,10]

III. EXPERIMENTAL RESULTS

Figures 4, 5, and 6 show cross sections from specimens tested in configurations 1, 2, and 3, respectively. The dark

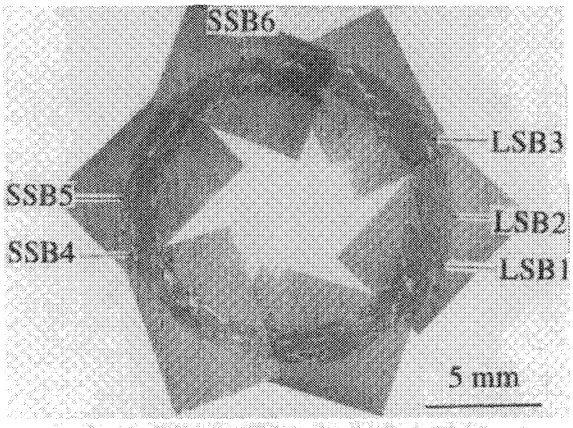

(*a*)

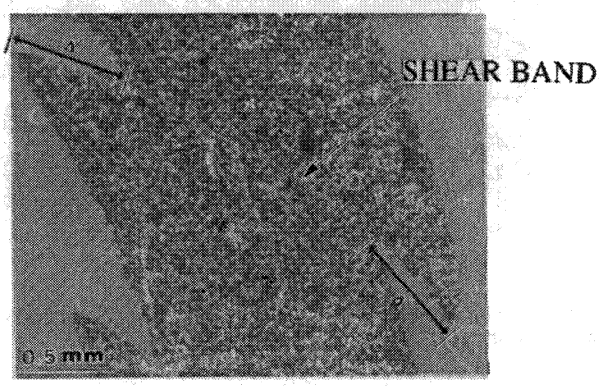

(*b*)

Fig. 4—Overall view of shear localization after cylinder collapse in configuration 1: (*a*) and (*b*) close-up of shear localization region (LSB1) with displacements Δ' and Δ on internal and external surfaces, respectively.

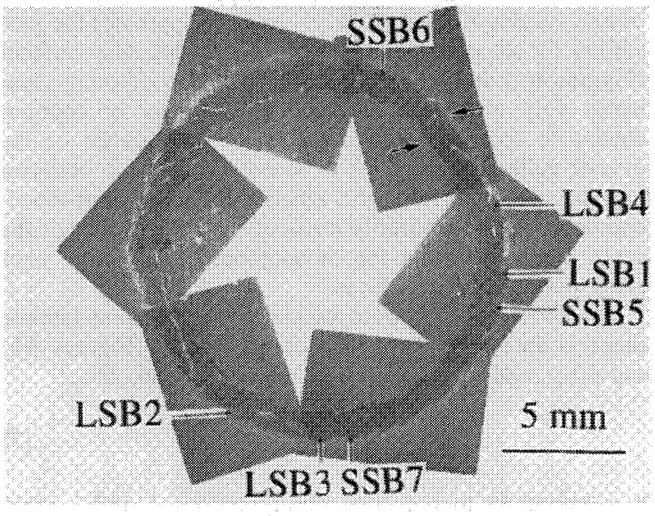

Fig. 5—Overall view of shear localization after cylinder collapse in configuration 2 with shear assistance by amorphous layer (shown by arrows).

ribbon on the external surface of the powder for configuration 2 (Figure 5) is the metallic glass. The nonhomoge-

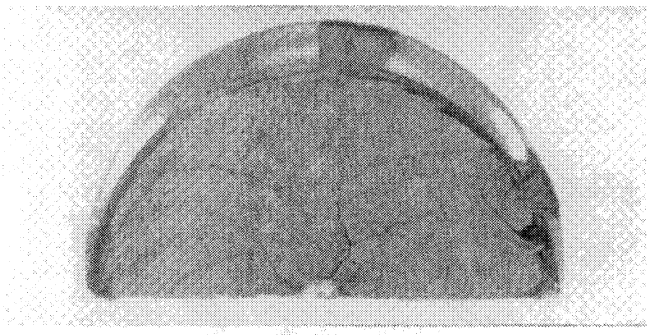

(*a*)

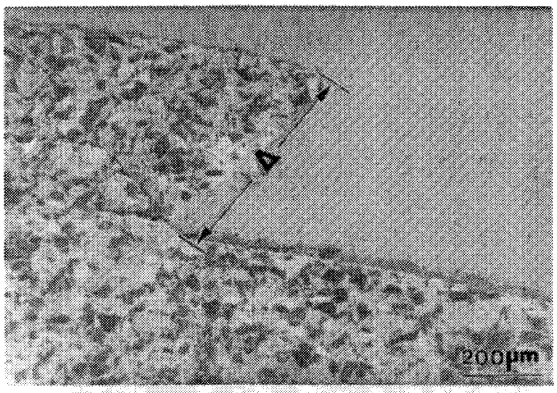

(*b*)

Fig. 6—(*a*) Shear bands for configuration 3 and (*b*) detail of single shear band near the container tube.

neous nature of the plastic deformation of the porous mixture is evident. The marks on Figures 4(a) and 5 show the shear bands analyzed. The shear localization regions make an angle of approximately 45 deg with the radius (direction of maximum shear stress for uniform stage of deformation (Figure 3)). It is interesting to mention that as in the case of metals,[8,9,10] in these experiments, the activity of one system of shear surfaces usually suppresses the possibility for shear development along perpendicular surfaces (Figures 4(a) and 5). The orientations of neighboring shear bands very often coincide (either clockwise or counterclockwise spirals). This indicates the importance of the overall collective behavior of shear bands. This behavior may be connected with the kinetics of shear band development: the first arbitrarily created shear band changes the stress state, inhibiting the development of adjacent ones along perpendicular surfaces.

The overall shear strain inside the shear zone (simple shear) is the ratio of the amplitude of shear, Δ (Figures 4(b) and 6(b)), and the thickness of the shear band, δ:

$$\gamma \approx \frac{\Delta}{\delta} \qquad [3]$$

It is important to note that configurations 1 and 2 yield "uniform" shear localization with approximately equal displacements ($\Delta \approx \Delta'$) at inner and outer surfaces of the porous mixture in configurations 1 and 2 (Figures 4 and 5), as a result of relatively close overall strains (e_{rr} and $e_{\varphi\varphi}$) at r and r_1. The shear displacements are in the range $\Delta \sim 100$ to 600 μm and the shear band thicknesses δ vary between 5 and 10 μm for configuration 1, 10 and 20 μm for configuration 2, and 10 and 40 μm for configuration 3. This enables the evaluation of shear strains according to Eq. [3]. The shear strains are found to be in the range of 10 to 100. For qualitative classification, shear bands with displacements Δ less than 10 maximal particle sizes in mixture (<400 μm) are called "small" shear bands (SSB) and those with larger displacements are called "large" shear bands (LSB). Both of them, which were analyzed, are correspondingly marked on Figures 4 and 5.

The kinematics of uniform overall deformation can be determined from the measurement of the inner surface velocity of the wall, V_i.[9] The radial and tangential strain rates for the homogeneous collapse of the cylinder are

$$\dot{e}_r = -\frac{(\rho^2 + R_0^2)^{1/2}}{(\rho^2 + R^2(t))^{3/2}} V_i(t)R(t), \qquad \dot{e}_{\varphi\varphi} = \frac{V_i(t)R(t)}{(\rho^2 + R_0^2)^{1/2}(\rho^2 + R^2(t))^{1/2}} \qquad [4]$$

where $V_i(t)$ and $R(t)$ are the time-dependent velocities of inner surface and radius of hole, respectively. It is assumed that the hole is fully closed in the collapse process (*i.e.*, $R = 0$) and that the collapse process is not significantly altered by the insertion of the porous material layer; therefore, measurements for copper cylinder were used. The overall mass of the copper driver was 24–38 times larger than the mass of the Nb-Si mixture, thus fully justifying this assumption. Strain rates, calculated from Eq. [4], on the basis of the measurements of $V_i(t)$, are represented in Figure 7 for configuration 2 for the inner and outer surfaces of the porous layer. It is important to note that the overall strain rates in these points are relatively close and are in the range (1.5 to 4) 10^4 s^{-1}, as in configuration 1.

The average shear strain rate inside the shear zone can be determined from the measurement of the time of the deformation process (time of pore collapse $\tau \approx 8$ μs)[9] and shear strain γ:

$$\dot{\gamma} \approx \frac{\gamma}{\tau} \qquad [5]$$

Shear strain rates are 10^6 to 10^7 s^{-1} for shear bands with different values of Δ, δ.

From the measurements of the inner surface velocity,[9] it is possible to calculate the inertial compression stress at the boundaries of the porous layer. The pressure distribution in a collapsing incompressible ideal liquid cylinder with zero pressure on its surfaces is expressed by[17]

$$p(\rho,R) = \frac{1}{2} d\, v_1^2 \left[\left(1 - \frac{R^2}{\rho^2}\right) - \left(1 - \frac{R^2}{R_1^2}\right)\frac{\ln(\rho/R)}{\ln(R_1/R)}\right] \qquad [6]$$

$$\left(\frac{\rho_m}{R}\right)^2 = \left(1 + \frac{R^2}{R_{10}^2 - R_0^2}\right)\ln\left(1 + \frac{R_{10}^2 - R_0^2}{R^2}\right)$$

where d is the density, ρ is the radius of one point inside the cylinder, v_1 is the current velocity of the inner surface, and ρ_m is the radius corresponding to the pressure maximum when the radius of the internal hole is equal to R (initial R_0) and the outer radius is R_1 (initial R_{10}). For the conditions of configurations 1 and 2 (initial velocity of inner surface 200 m/s), inertial compression stresses, calculated according to Eq. [6], are found to be less than 0.1 GPa. Thus, pressure effects can be neglected to a first approximation.

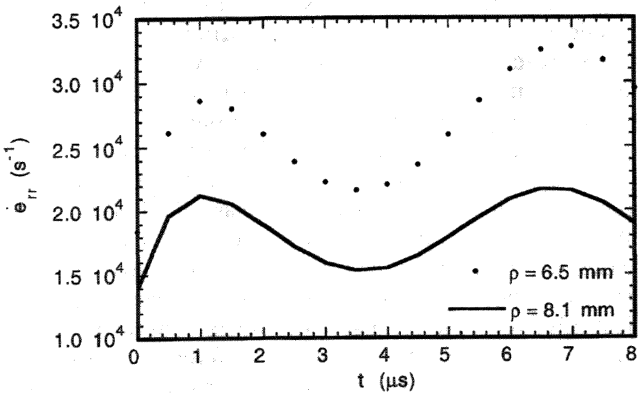

(*a*)

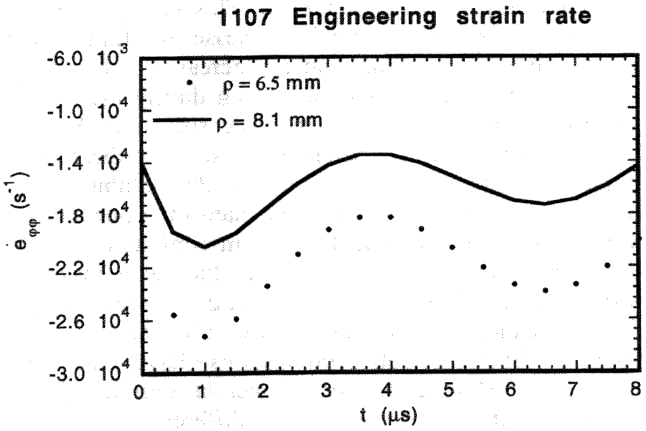

(*b*)

Fig. 7—Overall engineering strain rates ((*a*) $\dot{e}_{rr}$ and (*b*) $\dot{e}_{\varphi\varphi}$) for inner (ρ = 6.5 mm) and outer (ρ = 8.1 mm) surfaces of reactive porous cylindrical layer for configuration 2.

IV. DISCUSSION

It was demonstrated that densified Nb-Si and porous $MoSi_2$ + Mo + Si mixtures deform plastically, at high strain rates, by shear localization (configurations 1 and 3). Furthermore, it was possible to promote localized shear in a Nb- Si mixture (initially less dense than in configuration 1) by using a layer of metallic glass around the porous mixture (configuration 2).

The shear localization seems to result in the partial melting of one component (Si), as in shock-wave loading.[5,12,13] This is clear from the observations of typical cracks resulting from shrinkage during solidification at the boundaries of the shear bands and from the characteristic liquid flow of molten Si (dark material) in pores adjacent to shear bands (Figure 8). The small thickness of the shear band is responsible for quenching the material from the state resulting from localized plastic deformation and chemical reactions. The shear-band thickness has a tendency to increase with the decrease of the initial density of powder[11] and does not coincide with the initial particle size in the mixture. Taking the thermal diffusivity for the surrounding material as $k \sim 0.1$ cm^2/s, $\delta \approx 10$ μm, the quenching time τ_q, and quenching rate $\dot{T}$ are obtained:

$$\tau_q \sim \delta^2/\kappa \sim 10^{-5} \text{ s} \qquad [7]$$

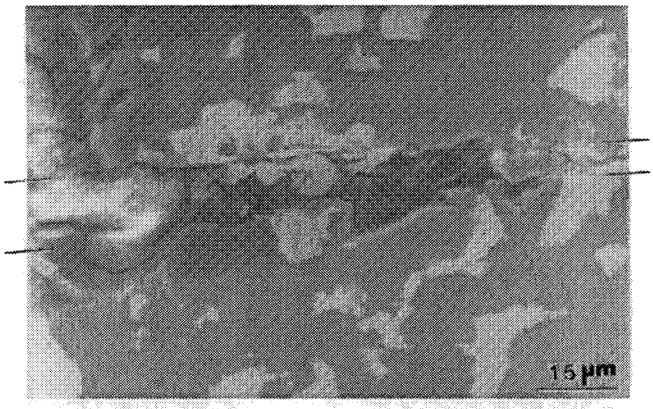

Fig. 8—Partial melting of Si inside the shear band for configuration 2.

$$\dot{T} \sim T/\tau_q \sim 10^8 \text{K/s} \qquad [8]$$

The small cooling time ensures retention of chemical reaction products formed during the deformation process.

The multiple fracturing of the Nb particles due to shear localization, at the mesolevel, leads to a decrease of the initial particle size from 44 to 0.1 to 2 μm and produces a unique fracture patterning inside the shear zone (Figure 9). Shear localization inside the Nb particles results not only in fracturing, but also in intense heating of the newly created thin particles. This is qualitatively different from the behavior of Nb particles in the mixture with Si in shock-wave compression with amplitudes up to 30 GPa[5–7,12,13] and is very important for triggering of chemical reactions.

Material flow inside the shear band is unstable and results in vortex formation. Evidence for vorticity, in the form of circular patterns by the split niobium particles, was found in configuration 1 (LSB4, Figure 10(a)) and configuration 2 (SSB5, Figure 10(b), and LSB5, Figures 10(c) and (d)). The arrows in Figure 10 show the regions where the thin layers, resulting from the shear fracture of the Nb particles (white), mark the rotations in the flow pattern. Vorticity can drastically enhance the heat and mass transfer. The minimum rotational frequency ω inside the vortex can be evaluated because the time for the process (τ = 8 10^{-6} s) is known, as is the number of circles. From these parameters, for one example (Figure 10(a), vortex diameter $\approx \delta/4 \approx 3$ μm), the corresponding rotational frequency is $\omega \sim 7\ 10^5$ s^{-1}. Patterning inside the shear zone due to either thermal or nonlocal effects (described by high-order gradient models) was recently predicted.[18,19] It is possible that vortex formation can be explained by a nonlocal mechanism: gradients in flow stresses due to the heterogeneity of the mixture are a possible cause.[19] An alternative explanation is based on hydrodynamic instability of the flow inside the shear zone. The upper limit of the Reynolds number, Re, for material flow inside the shear band can be evaluated assuming that the Si is completely molten. The overall average velocity V of flow can be calculated as

$$V \approx \Delta/\tau \qquad [9]$$

For $\Delta \approx 600$ μm and $\tau \approx 8$ μs, V is approximately equal to 75 m/s. The corresponding Reynolds number for the flow inside the shear band is

$$\text{Re} \approx V\,\delta/\nu. \qquad [10]$$

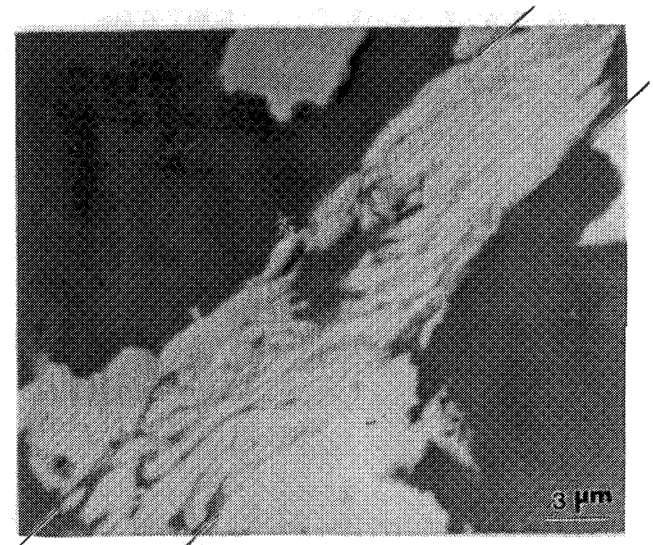

(*a*)

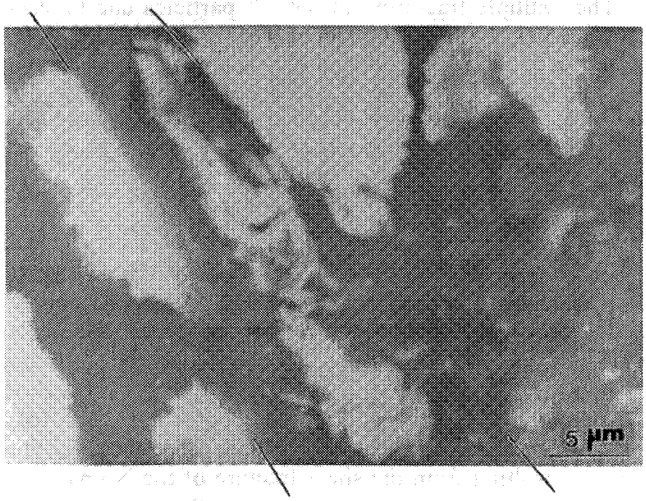

(*b*)

Fig. 9—(*a*) and (*b*) Fracture patterning of Nb particles inside shear bands (configuration 1); Nb is white, Si is dark, and the boundaries of shear band are shown by lines on the back.

Taking the viscosity value for pure liquid Si in the vicinity of the melting point $\nu \approx 0.4\ 10^{-2}$ cm^2/s[20] and $\delta \approx 10\ \mu$m, one obtains Re ≈ 1900. The hydrodynamic flow instability inside the shear band demands a critical Reynolds number between 3100 and 4000.[21] This can hardly be developed under these conditions, considering that the assumed viscosity of Si is the lower limit. In some cases, the vorticity was observed in regions with partial melting of Si and without the essential reaction between Nb and Si (Figure 10(b)). A viscosity of the partially molten amorphous Si at around 1000°C was estimated[22] to be $4 \times (10^3$ to $10^4)$ cm^2/s, giving Reynolds numbers six to seven orders of magnitude less than necessary for the beginning of turbulent flow in the geometry of observed shear bands. Nevertheless, this mechanism cannot be ignored, because material inside the shear band is not homogeneous and, therefore, the shear thickness is not uniform.

The intermetallic reaction between molten Si and fractured Nb proceeded in some regions (Figures 11(a) through (d)): the interior of cracks in Nb and small rounded particles inside Si with diameters less than 8 μm were favored sites. These reaction spots were identified by energy dispersive X-ray analysis. The analysis indicates that the reaction products shown in Figures 11(a) through (c) are Nb-rich phases (composition falls into the two-phase field of Nb_5Si_3 + $NbSi_2$) and that shown in Figure 11(d) is a Si-rich phase (composition corresponds to two-phase field $NbSi_2$ + Si). All of the reacted products have a rounded shape. In some cases, a central cavity can be seen, which provides experimental support for a liquid state of the reaction products just after reaction because the void is caused by solidification shrinkage. A qualitative difference between the shear-band structures for configurations 1 and 2 (having different initial densities) was observed. Reaction products with sizes up to 8 μm (Figures 11(a), (b), and (d)) were observed only for configuration 2. This can be explained by relatively larger shear band thicknesses resulting in more intense turbulent motions and an increase in the cooling time, as well as more intense heating during the uniform stage of deformation and essential densification. A higher initial powder density, resulting in smaller shear thicknesses, provides a faster cooling rate that inhibits the reaction in configuration 1. Another interesting phenomenon which should be mentioned is that in configuration 2, reaction products have approximately the same maximum sizes independent of the displacement Δ (Figures 11(a) and (b) correspond to LSB1, and Figures 11(c) and (d) correspond to -SSB5). Reaction products can have either a microdendritic (Figure 12) or a microcrystalline (Figures 11(b) through (d)) structure. The difference can be explained by local variations of element content and cooling rate. Very often, the reaction products were partially fragmented (Figures 11(a) and (d)) indicating that some deformation continued after the reaction was extinguished. At the same time, the absence of intense shear displacements (which were able to cut Nb particles (Figure 9)) clearly demonstrates that reaction products were formed after the main stage of shear deformation. In an analogy to the classification of chemical reactions resulting from shock loading by Thadhani,[7] the observed reactions can be called *shear-assisted* chemical reactions.

The dendritic structure of the reaction product with evident secondary dendrite arm spacings λ (Figure 12) enables the evaluation of cooling rate $\dot{T}$ (*K/s*). As dendrite coarsening on the stage of cooling can be neglected, λ can be used for calibrating very fast cooling rates by extrapolation from slower, well-determined cooling rates, using the relation[23]

$$\lambda \dot{T}^{1/3} = \text{const} \qquad [11]$$

The value of constant in Eq. [11] for the Nb-Si system is unknown, but for a qualitative evaluation, one can use the available data[22] for Al-7 to 11 wt pct Si for which const = 50 μm (K/s)$^{1/3}$. Using this value and $\lambda \approx 0.1\ \mu$m (Figure 12), one obtains $\dot{T} \approx 10^8$ K/s, which is in good agreement with the cooling rate calculated from the ratio of the temperature drop during cooling ($\sim 10^3$ K) and the previously estimated cooling time (based on the SSB thickness), which is close to the deformation process time (10^{-5} s). These evaluations confirm that despite the fact that reaction products (as can be concluded from their shape after deforma-

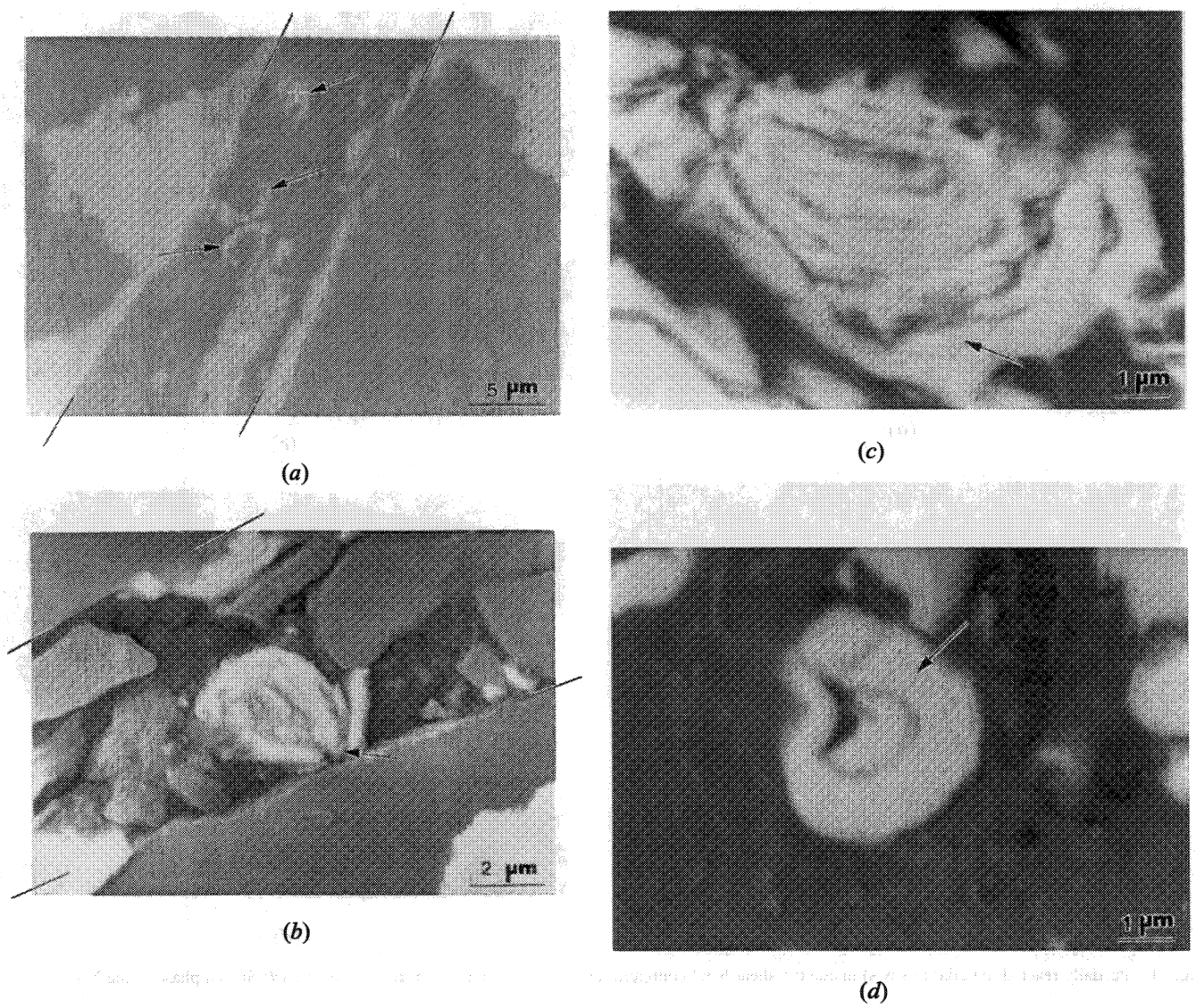

Fig. 10—Vortex formation (arrows) inside the shear band for (*a*) configuration 1 and (*b*) through (*d*) configuration 2.

tion) and the dendrites were formed after the main stage of the shear deformation, they nevertheless were formed in the same timescale of 10^{-5} s.

Configuration 3 provided broader and better defined reaction shear bands. The evidence of reaction is clear in Figure 13, corresponding to the initial mixture $MoSi_2$ + Mo + Si.[6,10] The white (Mo), black (Si), and gray ($MoSi_2$) regions outside of the shear zone are replaced by gray material inside it, showing that reaction between Mo and Si took place.

Reactions were not observed outside the shear zones for any of the configurations. These results are in accord with a recent report of shock-induced formation of $MgAl_2O_4$ spinel upon shock loading of single crystals (corundum-Al_2O_3 and periclase-MgO) by Potter and Ahrens.[24] In oblique impact experiments, up to a velocity providing a pressure in the 26 to 36 GPa range, reaction products were observed at the impact interface. It is probable that shear deformation also played an important role in these experiments.

The Nb-Si and Mo-Si systems have less propensity for initiation of shock-induced chemical reactions in comparison with Ti-Si and Ni-Si systems.[7] It was demonstrated in this research that reactions can be initiated by intense localized shear. The shear can be considered a promising tool for triggering reactions in other systems.

On the basis of the observations, a mechanism of shear-assisted chemical reaction leading to the product size with an order of magnitude close to the shear band thickness δ can be proposed. The main stages are as follows.

(1) Niobium particles are split into foils with thickness on the order of magnitude of (0.1 to 1) μm by localized mesoshears; small Nb particles with approximately the same sizes are also created as a result of this process. These foils and particles are heated as a result of intense shear deformation, which precedes their formation during plastic fracture, and have "fresh" surfaces, not contaminated by oxides.

(2) Silicon particles are molten and reaction begins due to the extensive relative flow of Nb particles and molten Si inside the shear band, in a similar manner to the mechanism proposed for shock-induced reactions.[3] The reaction proceeds along the Nb (sliver)—

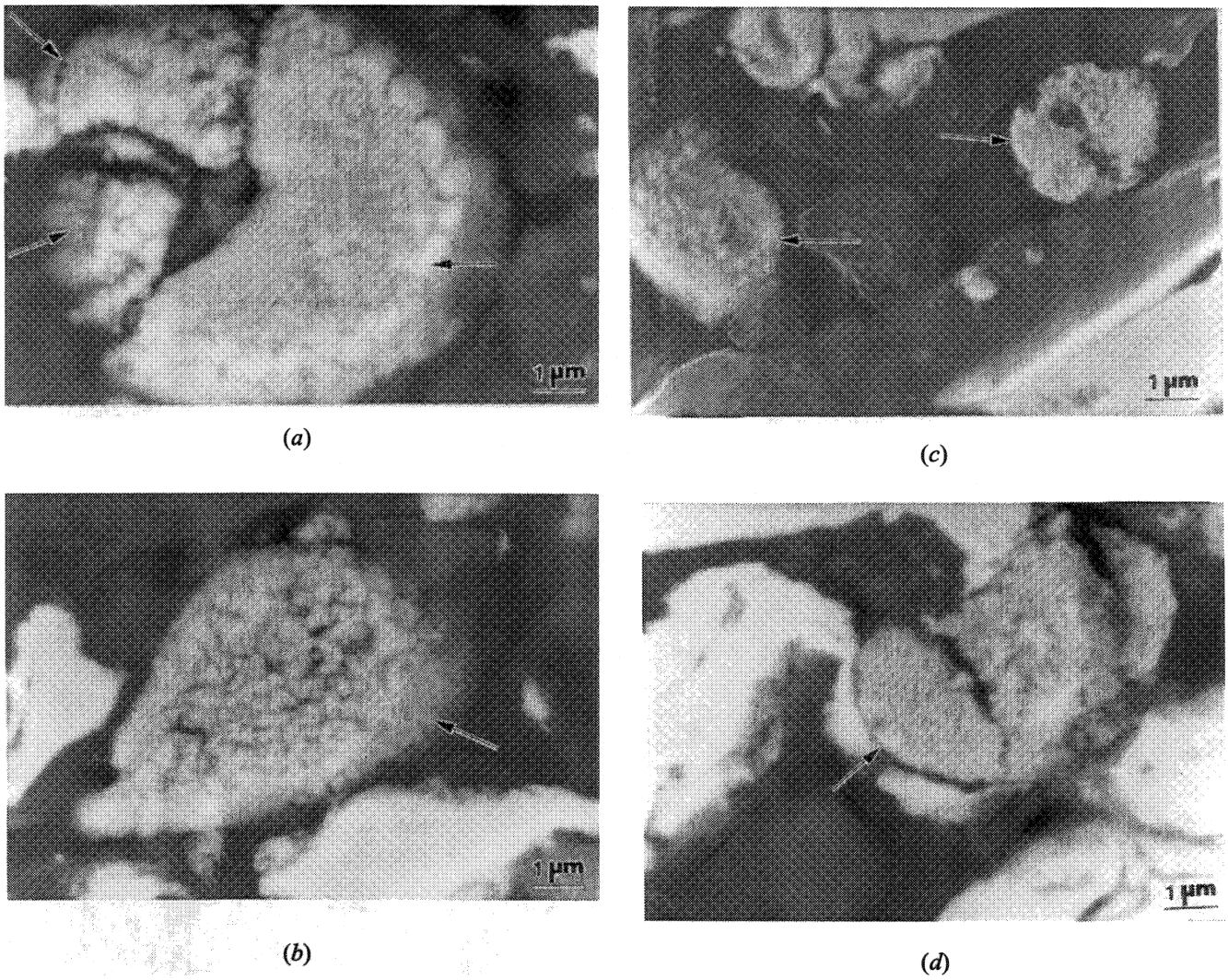

Fig. 11—Partially reacted material (arrows) inside the shear band configuration 2: (*a*), (*b*) and (*c*) Nb-rich phase and (*d*) Si-rich phase in the Nb-Si system.

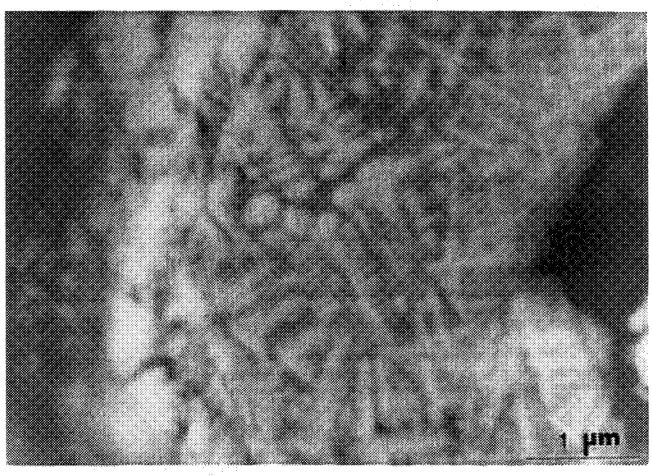

Fig. 12—Dendrite structure with secondary dendrite arm spacings $\lambda \approx 0.1$ μm; the reacted particle is the same one as in Fig. 8 (in the middle of the shear band) and in Fig. 11(a).

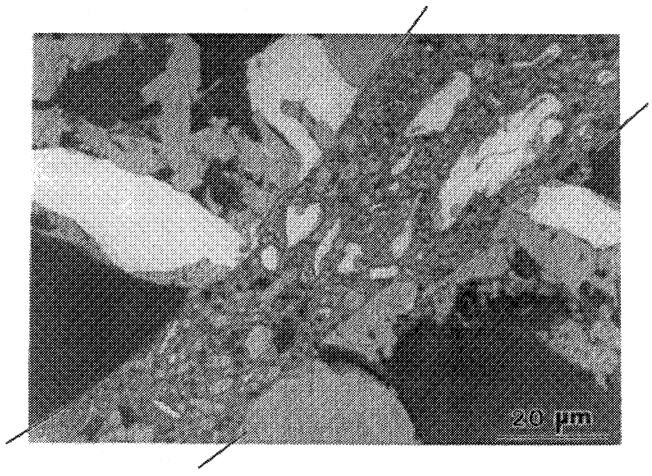

Fig. 13—Reacted shear band for configuration 3: $MoSi_2$ + Mo + Si system.

Si interface, with thickness l_r up to 1 μm size;[7] thus, the Nb sliver is at least partially transformed into the reaction product. The ROLLER model proposed by Dremin and Breusov[3] can be a possible mechano-chemical mechanism of reaction on this scale.

(3) Instability of gradient flow on another larger scale in-

side the shear band results in vorticity and the coiling of partially reacted Nb foils (as snow balls) together with adjacent Si into rounded particles with diameters up to 8 μm. Vorticity can also promote the collection of partially reacted small particles to the center of rotation, providing the typical size of reaction product on the order of 1 μm.

(4) Reaction continues up to the length D_r in places where temperatures are sufficiently high and is then quenched by thermal diffusion into the relatively cold surrounding material.

This mechanism enables the evaluation of the diameter of final reaction product, D_r, taking into account that it is equal to l_r, multiplied by the number of rotations in the vortex:

$$D_r \approx l_r \, \omega \, \tau \qquad [12]$$

The relations between V, δ, ω, and Δ are

$$\omega \approx \frac{V}{\delta}, \qquad \tau \approx \frac{\Delta}{V}, \qquad \gamma \approx \frac{\Delta}{\delta} \qquad [13]$$

Using Eqs. [12] and [13], an expression for the largest size of reaction product can be obtained in terms of the shear strain γ and reaction size l_r on the lower scale:

$$D_r \approx l_r \gamma \qquad [14]$$

Equation [14] clearly demonstrates that the size of the reaction product is proportional to the shear. For the current experiments, γ can be equal to 100, and this can provide the essential difference in scale between l_r and D_r. It is important to emphasize that Eq. [14] represents the connection between the size of the reaction region at the microlevel and the dimensions of the reacted particles at the macrolevel determined by the mechanical shear movement of material.

The analogous relation between sizes of reaction products can be applied between any adjacent structural levels (for example, between scale l_r and some lower level) if corresponding shear deformation exists on an upper scale. The main attributes of the mechanism are in qualitative agreement with the proposed phenomenological CONMAH model for shock-wave loading.[1]

V. CONCLUSIONS

The feasibility of the generation of controlled high-rate localized shear bands in heterogeneous, reactive porous materials has been demonstrated. The thick-walled cylinder method provides, in comparison with shock-wave loading, larger values of relative displacements of the reactant materials. The high rate shear, with overall parameters up to $\gamma = 100$ and $\dot{\gamma} = 10^7$ s^{-1}, results in the qualitative change of particle morphology (fracture of Nb particles) and melting of the lowest melting-point material (Si) with partial shear-assisted reaction in separate spots. A new mechanism of shear-assisted chemical reaction, qualitatively different from the one observed for shock-wave loading, is proposed. It predicts a linear dependence of the reaction product size on the shear strain if the conditions for shear flow instability are satisfied and the reaction takes place at the microscale.

ACKNOWLEDGMENTS

The authors would like to thank A. Molinari, K.S. Vecchio, and G.T. Gray for valuable discussions, R.J. Skalak for support, G. Velasco for help in manuscript preparation, and M.S. Hsu for metallography. This research is supported by the United States Army Research Office, Contract No. DAAH 04-94-G-031, United States Office of Naval Research, Contract No. N00014-94-1-1040, National Science Foundation, Grant No. MSS 90-21671, and the Institute for Mechanics and Materials, UCSD.

REFERENCES

1. R.A. Graham: *Solids under High Pressure Shock Compression: Mechanics, Physics and Chemistry*, Springer-Verlag, New York, NY, 1993.
2. S.S. Batsanov: *Effects of Explosions on Materials*, Springer-Verlag, New York, NY, 1993.
3. A.N. Dremin and O.N. Breusov: *Russ. Chem. Rev.*, 1968, vol. 37, pp. 392-402.
4. P.W. Bridgman: *Phys. Rev.*, 1935, vol. 48, pp. 825-47.
5. M.A. Meyers, L.-H. Yu, and K.S. Vecchio: *Acta Metall. Mater.*, 1994, vol. 42, pp. 715-29.
6. M.A. Meyers: *Dynamic Behavior of Materials*, John Wiley & Sons, Inc., New York, NY, 1994, pp. 222 and 640.
7. N.N. Thadhani: *J. Appl. Phys.*, 1994, vol. 76, pp. 2129-38.
8. V.F. Nesterenko, A.N. Lazaridi, and S.A. Pershin: *Fiz. Goreniya Vzryva*, 1989, vol. 25, pp. 154-55 (in Russian).
9. V.F. Nesterenko, M.P. Bondar, and I.V. Ershov: in *High-Pressure Science and Technology—1993*, S.C. Schmidt, J.W. Shaner, G.A. Samara, and M. Ross, eds., AIP Press, New York, NY, 1994, pp. 1173-76.
10. V.F. Nesterenko and M.P. Bondar: *DYMAT J.*, 1994, vol. 1, pp. 245-51.
11. V.F. Nesterenko, M.A. Meyers, H.C. Chen, and J.C. LaSalvia: *Appl. Phys. Lett.*, 1994, vol. 65, pp. 3069-71.
12. K.S. Vecchio, L.-H. Yu, and M.A. Meyers: *Acta Metall. Mater.*, 1994, vol. 42, pp. 701-14.
13. L.H. Yu, W.J. Nellis, M.A. Meyers, and K.S. Vecchio: in *High-Pressure Science and Technology—1993*, S.C. Schmidt, J.W. Shaner, G.A. Samara, and M. Ross, eds., AIP Press, New York, NY, 1994, pp. 1291-94.
14. S.A. Pershin and V.F. Nesterenko: *Combust., Explos. Shock Waves*, 1989, May, pp. 752-55.
15. M.A. Meyers and S.L. Wang: *Acta Metall. Mater.*, 1988, vol. 36, pp. 925-36.
16. A.E.H. Love: *A Treatise on the Mathematical Theory of Elasticity*, 4th ed., Dover Publishing, New York, NY, 1944, pp. 33-34.
17. H. Knoepfel: *Pulsed High Magnetic Fields*, North-Holland Publishing, London, 1970, pp. 206-09.
18. A. Molinari and Y.M. Leroy: *C.R. Acad. Sci. Paris*, 1991, Ser. 2, vol. 313, pp. 7-13.
19. Y.M. Leroy and A. Molinari: *J. Mech. Phys. Sol.*, 1993, vol. 41, pp. 631-63.
20. *Metals Reference Book*, 5th ed., Colin J. Smithells, ed., Butterworth and Co., London, 1976, p. 945.
21. H.L. Dryden, F.D. Murnaghan, and H. Bateman: *Hydrodynamics*, Dover Publishing, New York, NY, 1956, p. 345.
22. Y. Masaki, Q. Wei-Feng, M. Suzuki, and A. Kitagawa: *Jpn. J. Appl. Phys.*, 1994, Part 2 (Letters), vol. 33, pp. L1019-L1022.
23. R.W. Cahn: in *Physical Metallurgy*, 3d ed., R.W. Cahn and P. Haasen, eds., Elsevier Science Publishers BV, Amsterdam, 1983, Part 2, pp. 1779-1852.
24. D.K. Potter and T.J. Ahrens: *Geophys. Res. Lett.*, 1994, vol. 21, pp. 721-24.